UDC 539.3 DOI: 10.32326/1814-9146-2022-84-4-468-479

COMPARATIVE ANALYSIS 2: MULTISCALE MECHANISMS OF DEFORMATION AND FRACTURE UNDER HIGH-VELOCITY PENETRATION

Meshcheryakov Yu.I.[1], **Divakov A.K.**[1], **Zhigacheva N.I.**[1], **Konovalov G.V.**[1], **Osokin E.P.**[2]

[1]*Institute for Problems of Mechanical Engineer in RAS, Saint-Petersburg, Russian Federation*
[2]*Central Research Institute of Constructional Materials "Prometei", Saint-Petersburg, Russian Federation*

ym38@mail.ru

Received by the Editor 2022/05/29

Two kinds of aluminum alloy, 1561 and 1565 alloys, were tested in parallel within impact velocity range of 250–750 m/s in two schemes of shock loading: (i) under uniaxial strain conditions and (ii) in high velocity penetration. Combination of load regimes allows a formation of multiscale structure to be retraced. In both schemes of dynamic loading, the transition into structure-unstable state and change of scale level of dynamic deformation was found to occur under identical impact velocities. Formation of mesoscale-1 (1–10 μm) for both alloys is found to be identical – the mesoscale-1 structures are nucleated due to particle velocity fluctuations resulting from interaction of shock front with the structural heterogeneities. The intensity of the velocity fluctuations is registered in real time in tests under uniaxial strain condition by using the interferometric technique. For the mesoscale-2 (50–150 μm), the formation of dynamic structures is studied by using microstructural data of post-shocked specimens. In 1561 alloy, the structural elements in the form of cell-structures of 50–150 μm are the result of collectivization of mesoscale-1 structures whereas in 1565 alloy the mesoscale-2 structures are the periodical fault-cellson the boundary of penetration cavern. The strength behavior of both kinds of aluminum alloys in different schemes of loading turns out to be opposite – where the resistance to penetration increases, the spall strength decreases.

Keywords: aluminum alloys, spallation, penetration, rotations, shear bands, faults-structures.

Introduction

Development of the multiscale mechanics of deformed solid supposes incorporating the intermediate scales between macroscale and microscale [1–3]. At least three scale levels of deformation have been recognized for over several decades: dislocation scale, mesoscale and macroscale. Shock wave experiments provide an additional information concerning fundamental processes governing material response at extreme conditions. Specifically, the dynamic deformation initiated by shock loading can be presented in form

of two-scale configuration including two sublevels – the mesoscale-1 (1–10 μm) and mesoscale-2 (50–500 μm) [4, 5]. The additional effects which raise serious concern are the phenomena followed by transient non-equilibrium processes [6–8]. In the present paper, a critical step in having an efficient picture of multiscale processes is the parallel tests in two schemes of shock loading. The first scheme is the test under uniaxial strain conditions [9, 10] and the second scheme is the high-velocity penetration of elongated rigid rod [11–14]. Combination of two schemes of dynamic loading allows the following problems of multiscale straining to be understood: (i) whether the scheme of loading affects the meso-macro transition; (ii) how the initial structure of material affects the resistance to spallation, on the one hand side, and resistance to penetration, on the another hand side, (iii) how above features depend on the intensity of meso-macro momentum exchange during the multiscale dynamic deformation.

1. Experimental technique

Equipment for tests under high-velocity penetration is identical that used for test under uniaxial strain conditions [15].To provide perpendicularity relatively plane target, the rod of 20 mm in length and 5 mm in diameter is mounted into poly-vinyl carbonate sabot (Fig. 1*a*). The conditions for «*rigid rod and target*» are provided by using the high-strength 02Cr18Co9Mo5-VI maraging steel as a material for rod [16]. The tests on penetration allow the evolution of structure to be retraced owing to post-shocked structural investigation of the targets loaded under different impact velocities (Fig. 1*b*). In our approach, the strain rate data for transition of materials into structure unstable state obtained under uniaxial strain conditions (plane impact tests in [15]) are compared with those obtained in penetration tests. In the first case, owing to fine focusing of laser beam up to 50–70 μm, the fringe signal of interferometer corresponds to response of single mesoscale-2 structural element. This means that used plane impact tests provide the studying of the *incipient stage* of dynamic deformation and fracture.

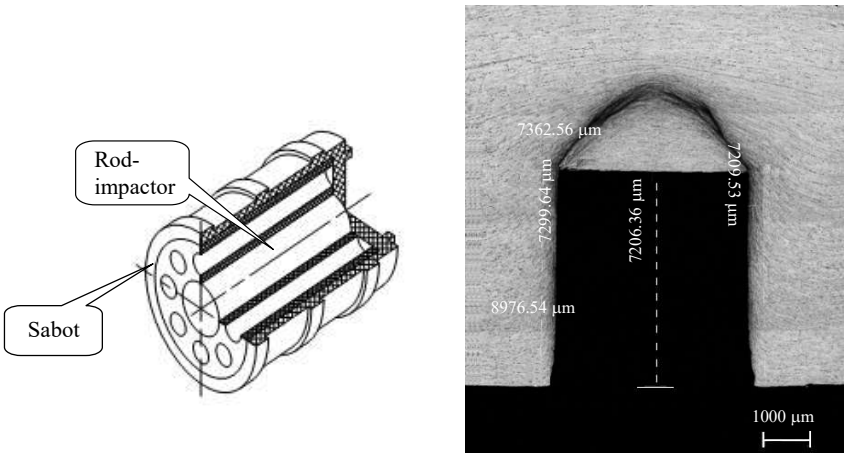

a) *b*)

Fig. 1. Poly-vinyl-carbonate sabot and steel rod-impactor (*a*);
penetration cavern in 1561 aluminum alloy at the impact velociy of 577 m/s (*b*)

Three dynamic characteristics can be registered in tests under uniaxial strain conditions. One of the basic characteristic of dynamic deformation which provides the quantitative

data on the intensity of energy and momentum exchange between scales is the *defect of particle velocity*. It's determined as a difference between velocity of impactor under symmetrical collision and maximum free surface velocity at the plateau of compressive pulse $U = (U_{\text{imp}} - U_{fs\,\max})$. In [15], in order to determine the instability threshold in plane impact tests, a set of identical targets for both alloys has been loaded within impact velocity range of 250–750 m/s.

In Fig. 2, the dependencies of maximum free surface velocity, $U_{fs\,\max}$, for 1561 and 1565 aluminum alloys are plotted as functions of impact velocity. The dash line corresponds to the equality of impact velocity under symmetrical collision and maximum free surface velocity ($U_{imp} = U_{fs\,\max}$). For 1565 aluminum alloy, the critical changes of slope for the maximum free surface velocity happen twice: at the impact velocity of 435 m/s (the free surface velocity equals 371.5 m/s) and at the impact velocity of 625.3 m/s (free surface velocity equals U_{ins} = 588.7 m/s. As for 1561 aluminum alloy, dependence $U_{fs\,\max} = f(U_{imp})$ does not contain the breaks. The maximum free surface velocity smoothly increases with the increasing of impact velocity.

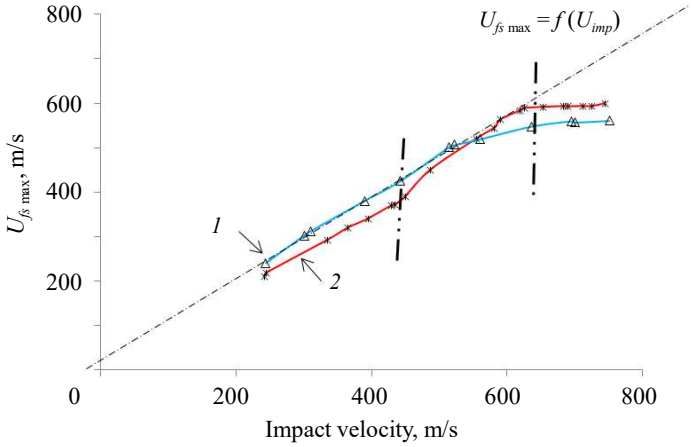

Fig. 2. Dependencies of maximum free surface velocity on impact velocity for 1561 (*1*) and 1565 (*2*) aluminum alloys

In the penetration tests, the only registered characteristic of loading is the impact velocity of rod. Resistance to high velocity penetration is characterized, firstly, by the value of penetration depth, L, and secondly, by the slope of curve $L = f(U_{imp})$: (i) the smaller penetration depth L, the higher resistance to penetration and (ii) the smaller the slope of curve $L = f(U_{imp})$, the higher the resistance to penetration.

2. 1565 Aluminum alloy: maximum free surface velocity, velocity defect, spallation and penetration

In Fig. 3 the dependencies of $U_{fs\,\max} = f(U_{imp})$ and penetration depth $L = f(U_{imp})$ are plotted.Within impact velocity range of 241.9–750 m/s, the penetration curve experiences the breaks at the impact velocities of 440 m/s (position B') and 625.5 m/s (position C'). The relation between rate of change of structural instability threshold and rate of change of penetration depth can be summering as following:

1) impact velocity region of 241.9–625.5 m/s: $dU^{AB}_{fs\,\max}/du < dU^{BC}_{fs\,\max}/du$, $dL_{A'B'}/du < < dL_{B'C'}/du$;

2) impact velocity region of 440–750 m/s: $dU^{CD}_{fs\max}/du < dU^{BC}_{fs\max}/du$, $dL_{C'D'}/du < dL_{B'C'}/du$.

The inequality $dL_{A'B'}/du < dL_{B'C'}/du$ means that resistance to penetration decreases after impact velocity of 440 m/s. Within impact velocity region from 625.5 to 750 m/s, after point C', an analogous inequality takes place: $dL_{C'D'}/du < dL_{B'C'}/du$, which means that resistance to penetration after impact velocity of 625.5 m/s increases as well.

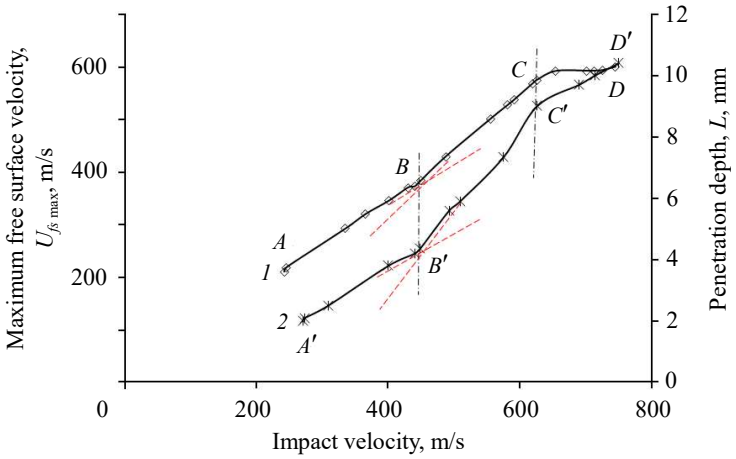

Fig. 3. Maximum free surface velocity $U_{fs\max}$, (*1*) and penetration depth, L, (*2*) versus impact velocity for 1565 aluminum alloy

The beaks for both curves happen at the identical impact velocities (indicated with vertical dotted lines). It may be concluded that the processes responsible for structural instability of material under plane impact tests and high velocity penetration are mutual related. In Fig. 4 the penetration depth curve $L = f(U_{imp})$ is plotted together with the dependence for velocity defect ΔU. Comparison of curves shows that correlation between processes really exists.The critical change of slope for penetration dependence happens just at the impact velocity where the break for dependence $\Delta U = f(U_{imp})$ occurs.

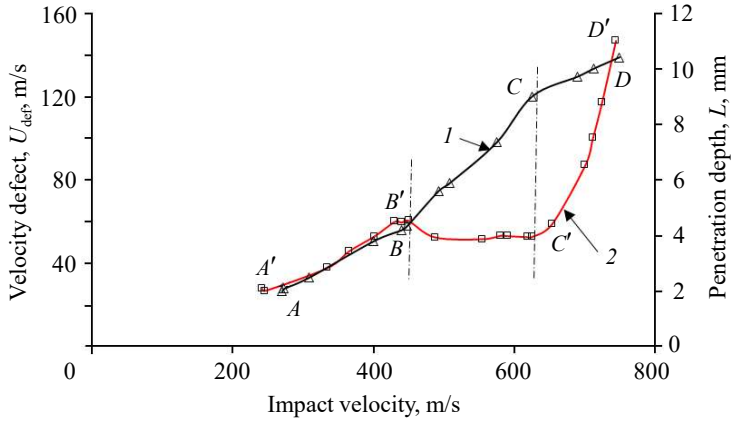

Fig. 4. Penetration depth, L (*1*), and velocity defect, ΔU(*2*) versus impact velocity

Dependence $\Delta U = f(U_{imp})$ determined in the tests under uniaxial strain conditions experiences two breaks: at the impact velocities of 440 m/s and 625.5 m/s. The dependence of penetration depth $L = f(U_{imp})$ also experiences two breaks: at the impact velocities of

440 m/s and 608 m/s. Such behavior of curves evidences the common mechanism of structure behavior in tests under uniaxial strain conditions and high velocity penetration.The breaks at high region of impact velocities in both loading schemes also happen at close impact velocities: 625.5 m/s in plane tests and 608 m/s in penetration tests. The relations between rate of change of velocity defect and rate of change of penetration depth can be summering as following:

1) impact velocity region of 241.9–625.5 m/s: $d\Delta U_{A'B'}/du > d\Delta U_{B'C'}/du$, $dL_{AB}/du < dL_{BC}/du$;

2) impact velocity region of 440–750 m/s: $d\Delta U_{C'D'}/du > d\Delta U_{B'C'}/du$, $dL_{CD}/du < dL_{BC}/du$.

Within upper region of impact velocities *CD*, the resistance to penetration increases. The beaks for both curves happen at the identical impact velocities (indicated with vertical dotted lines).

Now let us consider a correlation between spall strength behavior and resistance to penetration over the total impact velocity regions. Within impact velocity region of 241.9–625.5 m/s, the slope of penetration depth curve changes: $dL_{A'B'}/du < dL_{B'C'}/du$, which means that the resistance to penetration within impact region $A'B'$ of curve (*2*) is higher as compared to that for piece $B'C'$. At the same time, the spall strength *W* within the same impact velocity region shows the opposite trend. Within the piece *AB* the spall strength decreases from 137.8 m/s to 117.3 m/s. After point *B*, within piece *BC* $dW_{BC}/du < 0$, which means that spall strength is approximately constant. The critical changes in both curves happen at impact velocity of 440 m/s. Similar situation is seen after the second critical impact velocity of ~625.5 m/s – within piece $C'D'$ the slope of penetration curve (*2*) decreases: $dL_{C'D'}/du < dL_{B'C'}/du$, i.e. the resistance to penetration within region $C'D'$ increases whereas $dW_{CD}/du < 0$, which means that spall strength in this region of strain rates decreases. Thus, within impact velocity range of ~ (241.9–744.8) m/s the strength behavior of 1565 aluminum alloy in two schemes of shock loading turn out to be opposite – *when resistance to penetration increases*, *the spall strength decreases*.

In Fig 5, together with the spall strength *W*, the dependencies for velocity defect Δu and velocity variance, *D* on the impact velocity are provided. The breaks at curves happen at the identical impact velocities.

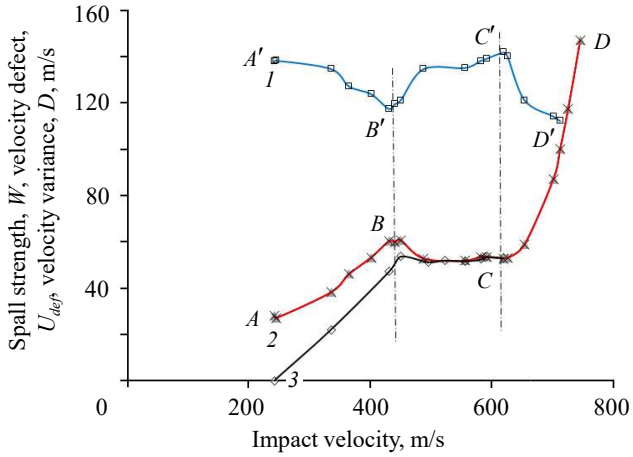

Fig. 5. Spall strength (*1*), velocity defect, (*2*) and velocity variance (*3*) versus impact velocity

The spall strength is seen to decrease when velocity defect increases (regions $A'B'$ and $C'D'$). At the same time both the spall strength and velocity defect are constant.

In [15], the non-monotonous behavior of spall strength has been analyzed from the position of macro-meso momentum exchange. In equilibrium case, when the rate of change of the velocity variance equals to rate of change of mean particle velocity $dD/dt = dU/dt$, the velocity defect equals to velocity variance $\Delta U = D$. This condition corresponds to situation when the local strain rate equals to macroscopic strain rate. Just these conditions are accomplished in the middle region of impact velocities $B'C'$ in Fig. 5. In shock-wave experiments, the local strain rate cannot be determined whereas the velocity defect and velocity variance are determinable. This allows the optimum regimes of dynamic deformation to be easily determined in experiments under uniaxial strain conditions in order to recommend for optimum regimes of utilizing a concrete material in penetration.

To understand the multiscale mechanisms of strength behavior of alloy in different regions of impact velocities it thought to be appropriately to compare the microstructural data for different regions of impact velocity with the dependencies of penetration length over the same regions. In our experiments, the post-shocked targets were cut along the impact direction and after polishing and etching in concentrated mixture of sulphuric and nitrogen asides were investigated with Axio-Observier Z-1m microscope.The initial structure of 1565 aluminum alloy contains the elongated grains, i.e. texture (Fig. 6*a*). The main feature of post-shocked specimens is a presence numerous microshears of 3–10 μm oriented along the shock direction. The shock-induced microshears have previously been studied in [17–19].

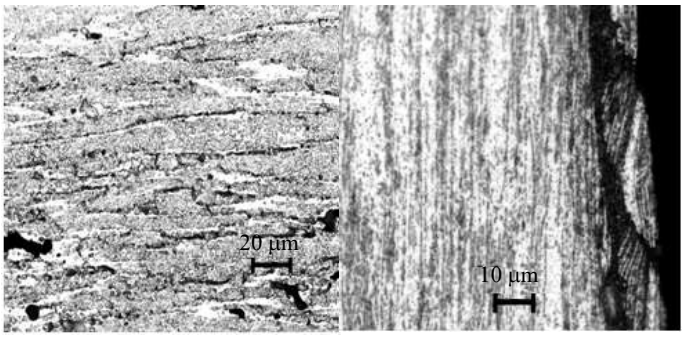

a) *b*)

Fig. 6. Initial structural states of 1565 aluminum alloy (*a*), microshears and fault structures in post shocked specimen (*b*)

In shock-wave experiments, the local strain rate cannot be determined whereas the velocity defect and velocity variance are determinable. This allows the optimum regimes of dynamic deformation to be easily determined in experiments under uniaxial strain conditions in order to recommend for optimum regimes of utilizing a concrete material in penetration. In our experiments, the post-shocked targets were cut along the impact direction and after polishing and etching in concentrated mixture of sulphuric and nitrogen asides were investigated with Axio-Observier Z-1m microscope. The initial structure of 1565 aluminum alloy contains the elongated grains, i.e. texture (Fig. 6*a*). To understand the multiscale mechanisms of strength behavior of alloy in different regions of impact velocities it thought to be appropriately to compare the microstructural data for different regions of impact velocity with the dependencies of penetration length over the same regions.

The main feature of post-shocked specimens is a presence numerous microshears of 3–10 μm oriented along the shock direction. Investigations of multiscale mechanisms of dynamic deformation in [20, 21] show that the behavior of mesostructure under dynamic loading can be characterized by presence of short-living pulsations of particle velocity of $\Delta t \approx$ 150–200 ns duration. The velocity interferometer registers the particle velocity distribution in form of velocity variance D. In the case of 1565 aluminum alloy, maximum value of velocity variance at the mesoscale-1 equals $D = 4.5 \cdot 10^3$ cm/s, from where the mean displacement equals: $L = D \cdot \Delta t = 4.5 \cdot 10^3 \cdot 2 \cdot 10^{-7} = 9 \cdot 10^{-4}$ cm. The displacements belong to mesoscale-1 (1–10 μm). Another structural element proper to high velocity penetration of 1565 aluminum alloy is the so-called fault-structures at the bank of cavern. In Fig. 6*b*, a complex morphology of fault-structure is presented – inside each fault-cell a family of shear bands is seen.

In Fig. 7, the states of structure for different regions of impact velocity indicated in Fig. 5 are provided. Within the regions *AB* and *CD*, the specific feature of post shocked specimens is the presence of regular fault structures near the bank of cavern and uniform deformation picture inside the region *BC*. Width of the region occupied by fault-structures depends on impact velocity: within region *AB* the width of fault structure zone equals 7–12 μm whereas at the region *CD* the width of the zone increases up to 47–50 μm. Comparison with the deformation regions for high velocity penetration curve (see Fig. 4) shows that resistance to penetration within regions *AB* and *CD* increases. Within region BC where the regular fault-cells are absent the post-shocked structure is uniform whist the resistance to penetration decreases. From the point of view of resistance to penetration, the 1565 aluminum alloy turns out to be more preferable at upper region of impact velocities where as the spall strength of 1565 alloy at the upper region of impact velocities decreases (see Fig. 5).

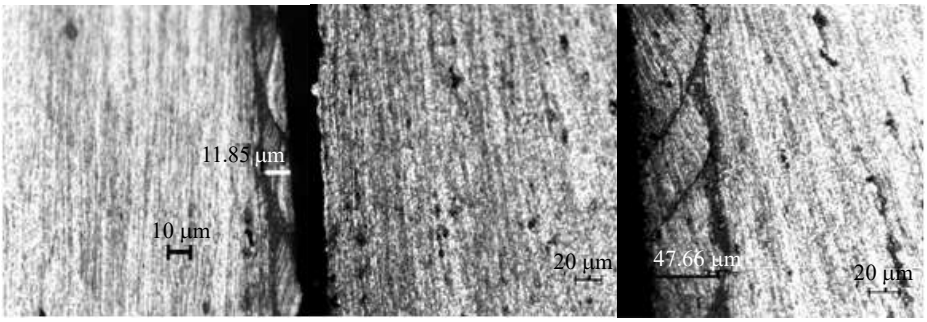

a) Region *AB* *b*) Region *BC* *c*) Region *CD*

Fig. 7. Three regions of lateral structure in 1565 aluminum alloy target after penetration

3. 1561 Aluminum alloy: spall strength and high-velocity penetration

In Fig. 8, the dependencies of maximum free surface velocity, $U_{fs\,\max}$, and penetration depth, L, on the impact velocity for 1561 aluminum alloy are plotted together. In this material the penetration depth gradually increases with the increasing of impact velocity.

Such behavior of the 1561 alloy becomes clear on the basis of microstructural investigations of post-shocked specimens. Initial state of grain structure for 1561 aluminum alloy is presented in Fig. 9*a*. The inner structure is seen to consists of equal-axis grains with the seldom inclusions of intermetallides. In Fig. 9*b* the morphology of lateral region

of cavern in 1561 alloy target loaded at the impact velocity of 328 m/s is shown. The numerous microshears oriented along the direction of impact are clearly seen. Nucleation of microshears evidences a transition to new kinematical mechanism of dynamic deformation – instead of uniform deformation, the deformation in form of shear banding at the mesoscale-1 is initiated. In vicinity of side wall of cavern, the distance between microshears decreases. The thickness of shear region increases with the increase of impact velocity from 40 μm at the impact velocities of 284 m/s to 100 μm at the velocity of 667 m/s.

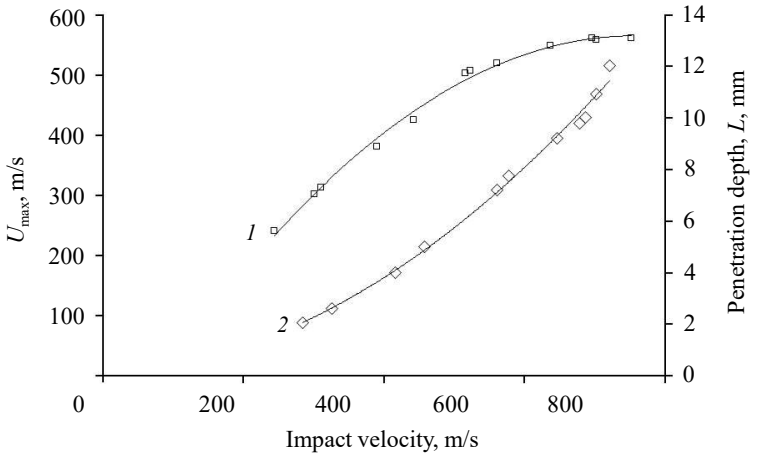

Fig. 8. Dependencies of maximum free surface velocity, $U_{fs\,max}$ (*1*), and penetration depth (*2*) on the impact velocity for 1561 aluminum alloy

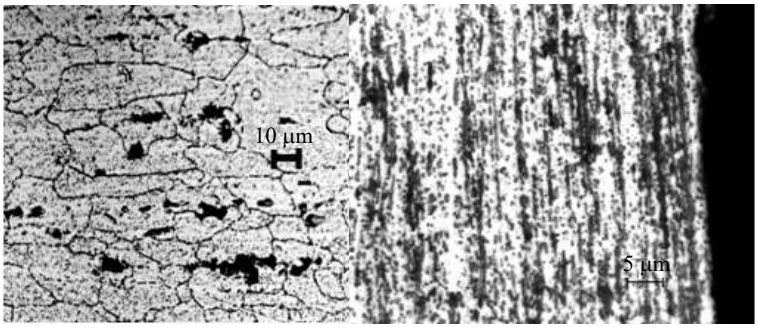

a) *b*)

Fig. 9. Initial structural states of 1561 aluminum alloy (*a*), longitudinal microshears (*b*) at the impact velocity of 328 m/s

With the increasing of impact velocity, the micro-shears unite into large-scale formations in the form of elongated plaits of 50–150 μm and cells in form of ellipsoids. In Fig. 10, such a type of formations are presented for different magnification. With the increasing of impact velocity, the region occupied by large-scale formations increases from 328.65 μm to 580 μm whilst the resistance to penetration is gradually decreases.

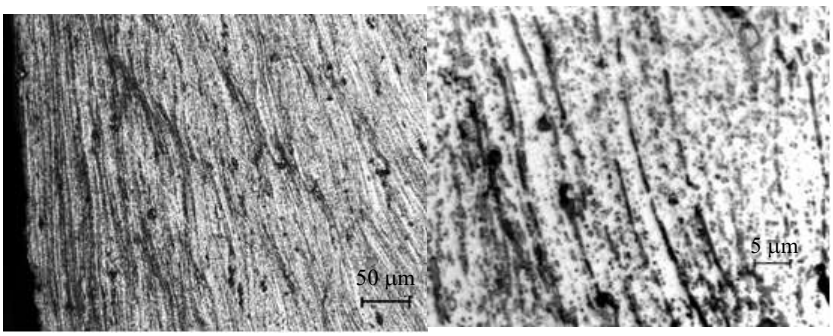

a) *b*)

Fig. 10. Structure of elongated plaits (*a*) and microshears in 1561 aluminum target at the impact velocity of 677 m/s (*b*)

Conclusions

As a results, it can be concluded.

Shock tests of 1565 and 1561 aluminum alloys in two schemes of loading reveal a correlation in threshold mechanisms of structural instability.

Formation of fault-structures in 1565 aluminum alloy increases the resistance to high velocity penetration.

Uniting of shear bands into elongated plaits and ellipsoids decreases the resistance to penetration.

The strength behavior of alloys in two schemes of loading proves to be opposite – when resistance to penetration increases, the spall strength decreases.

References

1. Panin V.E., Egorushkin V.E., Makarov P.V. *Fizicheskaya mezomekhanika i kompyuternoe konstruirovanie materialov* [*Physical Mesomechanics and Computer Modeling of Materials*]. In 2 vol. Vol 1. Novosibirsk. Nauka Publ. 1995. 298 p. (In Russian).

2. Panin V.E., Egorushkin V.E. Deformiruemoe tverdoe telo kak nelineynaya ierarkhicheski organizovannaya sistema [Deformable solid as a nonlinear hierarchically built system] *Fizicheskaya mezomekhanika* [*Physical Mesomechanics*]. 2011. Vol. 14. No 3. P. 7–26 (In Russian).

3. Panin V.E., Egorushkin V.E., Panin F.V. Fizicheskaya mezomekhanika deformiruemogo tverdogo tela kak mnogourovnevoy sistemy. I. Fizicheskie osnovy mnogomasshtabnogo podkhoda [Physical mesomechanics of deformed solid as multilevel system. I. Physical fundamentals of the multilevel approach]. *Fizicheskaya mezomekhanika* [*Physical Mesomechanics*]. 2006. Vol. 9. No 3. P. 9–22 (In Russian).

4. Meshcheryakov Yu.I., Divakov A.K., Zhigacheva N.I., Makarevich I.P., Barakhtin B.K. Dynamic structures in shock-loaded copper. *Phys. Rev. B*. 2008. Vol. 78. P. 64301–64316 DOI: 10.1103/PHYSREVB.78.064301.

5. Gupta Y.M. Shock wave experiments at different length scales: recent achievements and future challenges. Shock Compression of Condensed Matter-1999: Conference Proceedings. *AIP Conference Proceedings.* Snowbird, Utan (USA), 27 Jun–02 Jul. 1999. Vol. 505. No 3. 2000. P. 3–10. https://doi.org/10.1063/1.1303412.

6. Chhabildas L.C., Asay J.R. Rise-time measurements of shock transitions in aluminum,copper and steel. *J. Appl. Phys.* 1979. Vol. 50. Iss. 4. P. 2749–2756. https://doi.org/10.1063/1.326236.

7. Swan G.W., Duvall G.E., Thornhill C.K. On steady wave profiles in solids. *J. Mech. Phys. Solids.* 1973. Vol. 21. Iss. 4. P. 215–227. https://doi.org/10.1016/0022-5096(73)90021-5.

8. Davison L, Graham R.A. Shock compression of solids. *Phys. Rep*. 1979. Vol. 55. Iss. 4. P. 235–379. DOI: 10.1016/0370-1573(79)90026-7.

9. Cohran S., Banner D. Spall studies in uranium. *J. Appl. Phys*. 1977. Vol. 48. Iss. 7. P. 2729–2737. https://doi.org/10.1063/1.324125.

10. Grady D.E. The spall strength of condensed matter. *J. Mech. Phys. Solids*. 1988. Vol. 36. Iss. 3. P. 353–384. https://doi.org/10.1016/0022-5096(88)90015-4.

11. Flockhart C.J., Woodward R.L., Lam Y.C., O'Donnell R.G. The use of velocity discontinuities to define shear failure trajectories in dynamic plastic deformation. *Int. J. Impact Eng.* 1991. Vol. 11. Iss. 1. P. 93–106. DOI: 10.1016/0734-743X(91)90033-C.

12. Woodward R.L. Metallographic features associated with the penetration of titanium alloy targets. *Metall. Trans. A*. 1979. Vol. 10. Iss. 5. P. 569–573. DOI: 10.1007/BF02658319.

13. Woodward R.L. Modelling geometrical and dimensional aspects of ballistic penetration of thick metal targets. *Int. J. Impact Eng*. 1996. Vol. 18. No 4. P. 369–381.

14. Sternberg J., Orphal D.L. A note on the high velocity penetration of aluminum nitride. *Int. J. Impact Eng*. 1997. Vol. 19. No 7. P. 647–651.

15. Rosenberg Z., Dekel E. *Terminal Ballistics*. Heidelberg. London. New York. Springer. 2012. 326 p. DOI: 10.1007/978-3-642-25305-8.

16. Asay J.R., Chhabildas L.C. Determination of the shear strength of shock compressed 6061-T6 aluminum. In: Meyers M.A., Murr L.E. (eds.) *Shock Waves and High-Strain-Rate Phenomena in Metals: Concepts and Applications*. New York. Plenum Publishing Corporation. 1981. P. 417–431.

17. Murr L.E., Esquivel E.V. Review observation of common microstructural issues associated with dynamic deformation phenomena: twins, microbands, grain size effects, shear bands and dynamic deformation re-crystallization. *J. Mater. Sci.* 2004. Vol. 39. P. 1153–1168.

18. Grady D.E., Asay J.R. Calculation of thermal trapping in shock deformation of aluminum. *J. Appl. Phys*. 1982. Vol. 53. Iss. 1. P. 7350–7354. DOI: 10.1063/1.330101.

19. Meshcheryakov Yu.I., Prokuratova E.I. Kinetic theory of continuously distributed dislocations. *Int. J. Solids Struct*. 1995. Vol. 32. No 12. P. 1711–1726.

20. Prokuratova E.I., Indeitzev D.A. The conditions for the dislocation distribution localization under dynamic loading. *Dymat Journal*. 1995. Vol. 2. No 3/4. P. 229–233.

Список литературы

1. Панин В.Е., Егорушкин В.Е., Макаров П.В. *Физическая мезомеханика и компьютерное конструирование материалов*. В 2 т. Т. 1. Новосибирск: Наука. Сибирская издательская фирма РАН, 1995. 298 с.

2. Панин В.Е., Егорушкин В.Е. Деформируемое твердое тело как нелинейная иерархически организованная система. *Физическая мезомеханика*. 2011. Т. 14. №3. С. 7–26.

3. Панин В.Е., Егорушкин В.Е., Панин Ф.В. Физическая мезомеханика деформируемого твердого тела как многоуровневой системы. I. Физические основы многомасштабного подхода. *Физическая мезомеханика*. 2006. Т. 9. №3. Р. 9–22.

4. Meshcheryakov Yu.I., Divakov A.K., Zhigacheva N.I., Makarevich I.P., Barakhtin B.K. Dynamic structures in shock-loaded copper. *Physical Review B*. 2008. Vol. 78. P. 64301–64316. DOI: 10.1103/PHYSREVB.78.064301.

5. Gupta Y.M. Shock wave experiments at different length scales: recent achievements and future challenges. Shock Compression of Condensed Matter-1999: Conference Proceedings. *AIP Conference Proceedings*. Snowbird, Utan (USA), 27 Jun–02 Jul. 1999. Vol. 505. No 3. 2000. P. 3–10. https://doi.org/10.1063/1.1303412.

6. Chhabildas L.C., Asay J.R. Rise-time measurements of shock transitions in aluminum,copper and steel. *Journal of Applied Physics*. 1979. Vol. 50. Iss. 4. P. 2749–2756. https://doi.org/10.1063/1.326236.

7. Swan G.W., Duvall G.E., Thornhill C.K. On steady wave profiles in solids. J*ournal of the Mechanics and Physics of Solids*. 1973. Vol. 21. Iss. 4. P. 215–227. https://doi.org/10.1016/0022-5096(73)90021-5.

8. Davison L, Graham R.A. Shock compression of solids. *Physics Reports*. 1979. Vol. 55. Iss. 4. P. 235–379. DOI: 10.1016/0370-1573(79)90026-7.

9. Cohran S., Banner D. Spall studies in uranium. *Journal of Applied Physics*. 1977. Vol. 48. Iss. 7. P. 2729–2737. https://doi.org/10.1063/1.324125.

10. Grady D.E. The spall strength of condensed matter. *Journal of the Mechanics and Physics of Solids*. 1988. Vol. 36. Iss. 3. P. 353–384. https://doi.org/10.1016/0022-5096(88)90015-4.

11. Flockhart C.J., Woodward R.L., Lam Y.C., O'Donnell R.G. The use of velocity discontinuities to define shear failure trajectories in dynamic plastic deformation. *International Journal of Impact Engineering.* 1991. Vol. 11. Iss. 1. P. 93–106. DOI: 10.1016/0734-743X(91)90033-C.

12. Woodward R.L. Metallographic features associated with the penetration of titanium alloy targets. *Metallurgical Transactions A*. 1979. Vol. 10. Iss. 5. P. 569–573. DOI: 10.1007/BF02658319.

13. Woodward R.L. Modelling geometrical and dimensional aspects of ballistic penetration of thick metal targets. *International Journal of Impact Engineering*. 1996. Vol. 18. No 4. P. 369–381.

14. Sternberg J., Orphal D.L. A note on the high velocity penetration of aluminum nitride. *International Journal of Impact Engineering*. 1997. Vol. 19. No 7. P. 647–651.

15. Rosenberg Z., Dekel E. *Terminal Ballistics*. Heidelberg–London–New York: Springer, 2012. 326 p. DOI: 10.1007/978-3-642-25305-8.

16. Asay J.R., Chhabildas L.C. Determination of the shear strength of shock compressed 6061-T6 aluminum. In: Meyers M.A., Murr L.E. (eds.) *Shock Waves and High-Strain-Rate Phenomena in Metals: Concepts and Applications*. New York. Plenum Publishing Corporation. 1981. P. 417–431.

17. Murr L.E., Esquivel E.V. Review observation of common microstructural issues associated with dynamic deformation phenomena: twins, microbands, grain size effects, shear bands and dynamic deformation re-crystallization. *Journal of the Material Science.* 2004. Vol. 39. P. 1153–1168.

18. Grady D.E., Asay J.R. Calculation of thermal trapping in shock deformation of aluminum. *Journal of Applied Physics*. 1982. Vol. 53. Iss. 1. P. 7350–7354. DOI: 10.1063/1.330101.

19. Meshcheryakov Yu.I., Prokuratova E.I. Kinetic theory of continuously distributed dislocations. *International Journal of Solids and Structures*. 1995. Vol. 32. No 12. P. 1711–1726.

20. Prokuratova E.I., Indeitzev D.A. The conditions for the dislocation distribution localization under dynamic loading. *Dymat Journal*. 1995. Vol. 2. No 3/4. P. 229–233.

СРАВНИТЕЛЬНЫЙ АНАЛИЗ 2: МНОГОМАСШТАБНЫЕ МЕХАНИЗМЫ ДЕФОРМИРОВАНИЯ И РАЗРУШЕНИЯ МАТЕРИАЛОВ ПРИ ВЫСОКОСКОРОСТНОМ ПРОНИКАНИИ

Мещеряков Ю.И.[1], **Диваков А.К.**[1], **Жигачева Н.И.**[1], **Коновалов Г.В.**[1], **Осокин Е.П.**[2]

[1]*Институт проблем машиноведения РАН, Санкт-Петербург, Российская Федерация*
[2]*ЦНИИ конструкционных материалов «Прометей», Санкт-Петербург, Российская Федерация*

ym38@mail.ru

Поступила в редакцию 29.05.2022

Проведены ударные испытания двух типов алюминиевых сплавов 1561 и 1565 в диапазоне скоростей 250–750 м/с по двум схемам нагружения: (1) испытания в условиях одноосной деформации (плоского соударения) и (2) в условиях высокоскоростного проникания удлиненных ударников. Сочетание режимов нагружения и типов материала позволило детально проследить за процессом формирования многомасштабной структуры, инициированной ударным нагружением. В обеих схемах ударного нагружения переход материала в структурно-неустойчивое состояние и изменение масштабного уровня динамического деформирования происходило при одинаковой скорости деформации. При этом формирование мезоуровня-1 для обоих сплавов оказалось идентичным – структуры мезоуровня-1 (размером 1–10 мкм) в виде полос локализованного сдвига зарождаются за счет флюктуаций массовой скорости, инициируемых при взаимодействии ударной волны со структурными неоднородностями. Процессы формирования динамических структур на мезоуровне-2 (50–150 мкм) изучались посредством микроструктурных исследований образ-

цов. В алюминии 1561 элементы мезо-2 структуры представляют собой ячейки, которые формируются за счет коллективизации элементов мезо-1 структур по всему объему динамически деформируемого материала, в то время как в сплаве 1565 элементы структур мезо-2 – это периодические сбросовые ячейки по краям каверны, образованной при проникании удлиненного ударника. Прочностное поведение материалов оказалось зависящим от схемы нагружения. В одном и том же диапазоне скоростей ударного нагружения в случае одноосной деформации откольная прочность падает, в то время как сопротивление высокоскоростному проникнию возрастает. И наоборот, в диапазоне скоростей ударника, где откольная прочность возрастает, сопротивление высокоскоростному проникнию падает.

Ключевые слова: алюминиевые сплавы, откольное разрушение, высокоскоростное проникание, полосы локализованного сдвига, сбросовые структуры.